ACS Catalysis

Research Article

pubs.acs.org/acscatalysis

Ring-Opening Reactions of Methylcyclopentane over Metal Catalysts, M = Pt, Rh, Ir, and Pd: A Mechanistic Study from First-Principles Calculations

Zhi-Jian Zhao,[†] Lyudmila V. Moskaleva,[‡] and Notker Rösch*[,†,§]

[†]Department Chemie and Catalysis Research Center, Technische Universität München, 85747 Garching, Germany

[‡]Institut für Angewandte und Physikalische Chemie, Universität Bremen, 28359 Bremen, Germany

[§]Institute of High Performance Computing, Agency of Science, Technology and Research, 1 Fusionopolis Way, #16-16 Connexis, Singapore 138632

Supporting Information

ABSTRACT: Using density functional calculations we studied the conversion of methylcyclopentane to its various ring-opening products, branched and unbranched hexanes, that is, 2-methylpentane and 3-methylpentane, as well as *n*-hexane. We examined four metal catalysts, M = Pt, Rh, Ir, and Pd, using slab models of flat M(111) and stepped M(211) surfaces, to describe terrace-rich large and defect-rich small M particles, respectively. As C−H bond activation and formation is rather independent of the particle structure, we focused on C−C bond scission which is expected to be structure sensitive. The barriers of C−C bond scission indeed vary from ∼20 kJ mol^{-1} to ∼140 kJ mol^{-1} on various sites of these metal surfaces. In general, lower activation energies were calculated for Rh and Ir surfaces, in agreement with the higher experimental activity of these two metals compared to Pt and Pd. From the calculated C−C bond breaking barriers, we were able to rationalize the selectivity toward different ring-opening products, as observed in experiments over the metal catalysts studied.

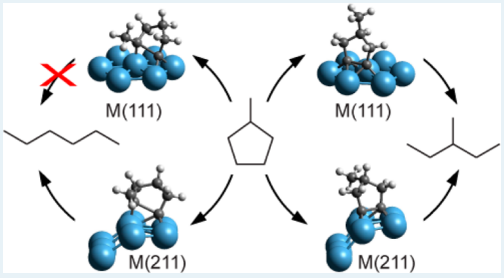

KEYWORDS: *ring-opening, methylcyclopentane, reaction mechanism, selectivity, noble metals, DFT calculations*

1. INTRODUCTION

Diesel fuels are among the most important and widely used energy sources currently available to power a wide variety of vehicles and operations. Although diesel-powered vehicles emit 10−20% less carbon dioxide than comparable gasoline vehicles,[1] diesel engine emissions contain more nitrogen oxides and carbonaceous particulate matter.[2] These pollutants are not only responsible for adverse environmental effects but also have a direct harmful impact on human health. Therefore, it is expected that in the near future even stricter limits will be placed on the content of nitrogen and polynuclear aromatics in diesel fuels as well as on the cetane number (CN), which is related to its aromatic content and provides a measure of the combustion quality of the fuel.[3] With modern upgrading technologies one is able to improve the CN of diesel fuels while concurrently reducing the content of aromatics.[4,5] In this process, the aromatic rings, which have low CN, need to be saturated and then cracked to form alkanes; ideally, only one endocyclic C−C bond per ring should be broken to avoid overcracking to lighter fragments. Among alkanes, isomers with smaller degree of branching are preferred because of their higher CN. Therefore, finding a way to selectively crack naphthenic is an important issue for modern petroleum industry.

Selective ring-opening (SRO) of naphthenes is catalyzed by supported noble metal particles and is thought to proceed via a bifunctional mechanism involving an isomerization of six-member hydrocarbon rings into five-member rings on (acidic) support, followed by ring cleavage on metal sites.[6] The ring-contraction step facilitates the overall conversion as direct cracking of six-member hydrocarbon rings is much harder than of five-member rings.[6−10]

Ring-opening (RO) of methylcyclopentane (MCP) on supported metal catalysts is a commonly employed model of SRO.[6,11−29] These studies were carried out using metals on neutral or active acidic supports. Note that RO can also take place directly on the support, yet with lower rates than on metal particles.[30] To decouple these two reaction venues, the present theoretical analysis focuses on the metallic function; hence we mainly comment on experimental studies that employed neutral supports. Three isomeric alkanes, 2-methylpentane (2MP), 3-methylpentane (3MP), and *n*-hexane (*n*Hx), can be produced via endocyclic C−C bond scission, at different positions relative to methyl substituent. The RO selectivity toward particular isomers depends on the nature of the metal catalyst. For example, the RO product distribution over Pt catalysts was shown in experiment to depend on the metal particle size.[18,19] Large Pt particles favor branched products,

Received: September 10, 2012
Revised: December 22, 2012
Published: January 14, 2013

2MP and 3MP,[18] which exhibit somewhat lower CN than the straight-chain product, *n*Hx. The selectivity toward *n*Hx increases on well-dispersed small Pt particles.[19] Some other metals, like Rh and Ir, showed higher activity compared to Pt,[12] but the distribution of the RO products obtained on these more active catalysts, irrespective of particle size, was selective toward branched hexanes instead of the straight-chain *n*Hx, preferred in terms of CN.[12,19−21,27] The distribution of the RO products catalyzed by Pd-based catalysts was reported to be stable with respect to the dispersion of the metal. The selectivity for *n*Hx on Pd was higher than on Rh and Ir, but still only half as large as statistical expectation.[22] Recent studies on bimetallic catalysts, for example, AuPt,[23] GePt,[15] RhPt,[12,24] RhGe,[25] also did not show any promising selectivity toward *n*Hx.

In the past several decades, extensive research focused on MCP RO. Yet, gaining detailed insight into the mechanism of this reaction by experiments alone was difficult because of the complexity of the chemistry involved. A number of mechanisms were proposed several decades ago,[7,18,26] and some of them, for example, the selective "dicarbene mechanism" or the non-selective "multiplet" mechanism, seem to have become widely accepted. However, experimental evidence directly confirming any particular mechanism is still lacking. Nowadays, computational studies based on the methods of density functional theory (DFT) provide tools for gaining a better understanding of elementary steps of complex reaction networks.[31−35]

Our recent study[36] proposed a detailed mechanism for RO of MCP based on the ideas of Gault et al. who decades ago suggested several dehydrogenation steps prior to an endocyclic C−C cleavage.[7,18] Accordingly, the conversion of MCP contains three major stages (Figure 1): (*i*) dehydrogenation of MCP, in the present case to an $\alpha\alpha\beta\beta$−tetra-adsorbed cyclic intermediate or an $\alpha\alpha\beta$−triadsorbed cyclic intermediate with a methyl substituent at β position, (*ii*) endocyclic C−C bond scission, and (*iii*) rehydrogenation to produce hexanes. The flat Pt(111) surface was chosen to represent large terrace-rich Pt particles while small defect-rich Pt particles were modeled by the stepped Pt(211) surface. Our study showed that on the Pt(111) surface the barrier for C−C bond breaking on the path to *n*Hx is significantly higher than the activation energies of the two pathways leading to branched products, 2MP and 3MP. This high barrier should inhibit the production of *n*Hx on large Pt particles which are expected to expose a large fraction of flat (111) facets. The results of our calculations are consistent with the experimental observation that large Pt particles preferentially produce branched 2MP and 3MP.[18] In contrast, on the stepped Pt(211) surface our calculations indicated a decrease of the high C−C scission barrier for *n*Hx formation to an energy similar to the rate-determining activation barriers leading to 2MP and 3MP at step-edge sites. This finding allowed one to rationalize why defect-rich small Pt particles primarily yield RO products in a statistical distribution.[19]

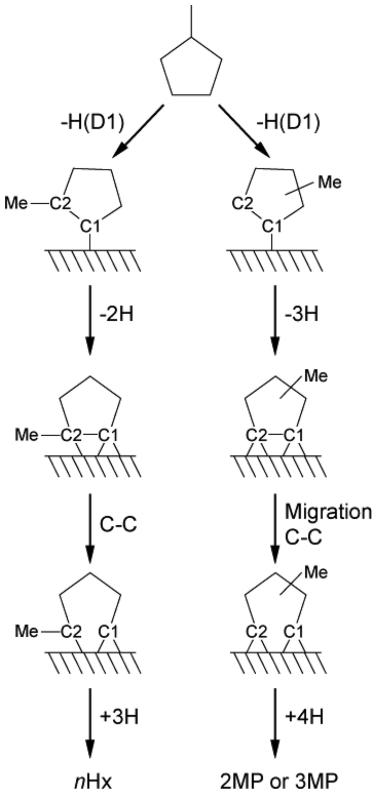

Figure 1. Set of reactions studied in this work.

To further explore this RO mechanism for MCP, we extended this research to three more metal catalysts, Rh, Ir, and Pd. All of them are active in MCP RO reactions, with the activity following the trend Ir ≈ Rh > Pt > Pd.[12] Similar to our previous study, we invoked two metal surfaces, flat M(111) and stepped M(211), to model metal particles of different sizes. The present work focused on C−C bond breaking which we found to be essential for interpreting the particle-size effect of Pt-based catalysts.[36] Our study attempts to rationalize the observed different activity and particle-size effects for the metal catalysts under discussion.

2. MODELS AND COMPUTATIONAL DETAILS

The calculations were carried out with the periodical DFT code Vienna ab initio simulation package VASP[37,38] using the generalized-gradient approximation PW91 for exchange-correlation functional.[39] We invoked the projector-augmented wave method[40,41] for describing the interaction between the valence electrons and the atomic cores. For the plane-wave basis we applied a cutoff energy of 400 eV. In the structure optimizations, the Brillouin zone was sampled with a Monkhorst-Pack mesh of 5 × 5 × 1 *k* points.[42] Subsequently the energy was refined with a 7 × 7 × 1 *k* point grid in a single-point fashion.[43−45] In all cases, we applied a first-order Methfessel-Paxton smearing with a width of 0.15 eV.[46] Finally, the total energies were evaluated by extrapolating to zero broadening.

The ideal M(111) and M(211) surfaces were represented by periodic slab models of five layers each, repeated in a supercell geometry with at least 1 nm vacuum spacing between them. The slab used to model the stepped surface M(211) comprises five layers of (111) orientation, but formally contains 15 layers perpendicular to the surface normal. During the optimization, the top two layers, together with the adsorbates, were allowed to relax until the force on each atom was less than 2×10^{-4} eV/pm. The other three "bottom" layers were kept fixed at the theoretical bulk-terminated geometry. We used a (3 × 3) unit cell for M(111) and a (3 × 1) unit cell for M(211), corresponding to surface coverage 1/9.

The dimer method[47] or the nudged elastic band (NEB) method[48,49] was used to determine the transition states (TS) of the reactions. In the latter case, six images of the system were employed to form a discrete approximation of the path in addition to the fixed end points. All optimized TS structures

dx.doi.org/10.1021/cs3005924 | ACS Catal. 2013, 3, 196−205

were checked by a normal-mode analysis to ensure that only one single mode exhibited an imaginary frequency.

The binding energy (BE) of an adsorbate was calculated from the energy difference between the total energy $E_{ad/sub}$ of the slab covered with the adsorbate in the optimized geometry and $E_{ad} + E_{sub}$, the sum of the total energies of the adsorbate in the gas phase (ground state) and the clean substrate, respectively:

$$BE = E_{ad} + E_{sub} - E_{ad/sub}$$

Positive values of BE imply a release of energy or a favorable interaction. Calculations on gas-phase hydrocarbon species with open shells were carried out in a spin-polarized fashion.

3. RESULTS

In the present study we assume the same RO mechanism as in our preceding study on Pt catalysts (Figure 1),[36] via an $\alpha\alpha\beta\beta-$tetra-adsorbed intermediate to form 3MP (2MP) and via an $\alpha\alpha\beta-$triadsorbed intermediate to form *n*Hx. C−C cleavage via less dehydrogenated intermediates is believed to be unlikely due to the high activation energy, for example, 148 kJ mol^{-1} for the RO of an $\alpha\beta-$diadsorbed intermediate on Pt(111).[36]

For RO on Pt(111),[36] we calculated the structures of intermediates and TSs for all elementary reaction steps, starting from MCP to the product hexane. We had demonstrated that the activation energies of all elementary steps on the reaction paths to 2MP and 3MP are very close to each other. Thus, only selected steps on the reaction pathways to 3MP and *n*Hx were calculated, and a statistical distribution 2MP:3MP = 2:1 was assumed on all metal surfaces studied (which is also close to the ratio observed in all cited experimental studies). In the following, when referring to the position of the methyl group within the ring, we shall denote, for convenience, the first C atom which binds to the metal surface as C1, and the second as C2; the other three carbon centers are numbered from C3 to C5 along the direction from C1 to C2.

3.1. Dehydrogenation Reactions. *First Dehydrogenation Step over M(111) Surfaces.* In the initial state (IS) of the first dehydrogenation step (D1), MCP is physisorbed over the metal surface M(111), where the C−H bond to be broken is oriented normal to the surface, directly on top of a metal atom (Figure 2). Because of the substituting methyl group, there are three unequal carbon atoms in MCP and three possibilities for D1. Accordingly, ISs with the methyl group attached to C1, C2 (∼ C5) or C3 (∼ C4) represent three alternative reaction paths. (Here C1 denotes the carbon center to be dehydrogenated first.) Our work on Pt(111)[36] showed that the activation energies of ±H reactions were not strongly affected by the position of the methyl substituent. Thus, we only considered two adsorption modes of MCP, with the methyl group attached to either C2 (C5) or C3 (C4). In this way, we checked that, also on the other three metal surfaces under consideration, D1 is not very sensitive to the position of the CH_3 substituent. These two of three possibilities for D1 would finally lead to three isomeric hexanes via the proposed mechanism.

First, we discuss the dehydrogenation reaction from the IS where the methyl group is attached to C3. The geometries of the ISs are quite similar on all (111) surfaces considered; see Figure 2a for an example. The ring backbone is approximately parallel to the surface showing weak H−M interactions. In the respective TSs, the adsorbate moves closer to the metal surface, forming a three-member ring structure C−H−M. In the final

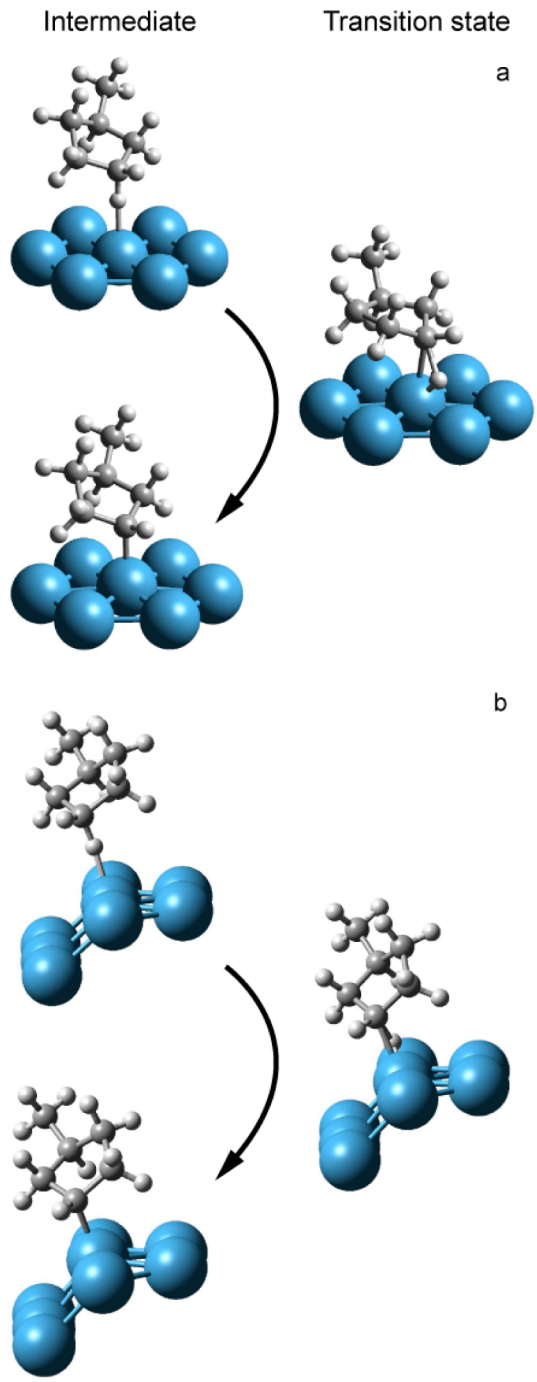

Figure 2. Optimized structures of the first dehydrogenation step on the reaction path to 3MP over (a) Pt(111), and (b) Pt(211).

state (FS), the hydrocarbon chemisorbs at a top site via a single C−M bond. The dissociated H atom is located at a 3-fold hollow site next to the hydrocarbon. For all metals considered, the activation energies of these dehydrogenation steps lie in the narrow range 79−90 kJ mol^{-1}. The reaction is thermoneutral over Pt(111) while on the other metal surfaces it was calculated endothermic by 23−33 kJ mol^{-1}.

Our earlier work on the Pt(111) surface[36] showed that the position of the methyl group does not have a large influence on the activation energy of a particular ±H reaction step. The same behavior is also observed over the other three metal surfaces (Table 1). For each of them, the barriers of the D1

dx.doi.org/10.1021/cs3005924 | ACS Catal. 2013, 3, 196−205

Table 1. Energy Characteristics (kJ mol^{-1}) of the Transition States Pertinent to the MCP RO Reactions over Pt(111) for Various Locations of the Methyl (Me) Substituent

			Pt		Pd		Ir		Rh	
final product	reaction step[a]	surface	ΔE^b	$E_a{}^c$	ΔE^b	$E_a{}^c$	ΔE^b	$E_a{}^c$	ΔE^b	$E_a{}^c$
3MP	D1	111	0	85	33	90	23	79	30	83
	D1	211	−3	50	19	60	−56	35	−13	49
	Migration (‖ to μ)	111	60	61	11	14	23	41	2	11
	Migration (‖ to μ)	211[d]			3	5	66	66	19	22
	CC (IS: μ-bridge)	111	−21	14	50	59	−20	17	5	16
	CC (IS: μ-bridge)	211[d]			76	84	−7	11	14	27
	CC (IS: ‖-bridge)	211[e]	40	102			15	89		
*n*Hx	D1	111	0	89	35	92	24	81	26	81
	D2	111	−17	65	−20	68	−6	45	−14	50
	D3	111	26	86	41	109	1	39	4	52
	CC	111	−19	116	4	134	−52	62	−49	70
	CC	211	12	94	58	119	−39	38	−7	59

[a]D*x* denotes the *x*th dehydrogenation step; CC refers to the C−C bond scission step. [b]Reaction energy. [c]Activation energy. [d]The reactions on Pt(211) do not contain this step. [e]The reactions on Rh(211) and Pd(211) do not contain this step.

step on the reaction path to *n*Hx (Me at C2 position) and to 3MP (Me at C3 position) differ at most by 4 kJ mol^{-1}.

First Dehydrogenation Step over M(211) Surfaces. As discussed above, the position of the methyl group is not expected to affect the activation barrier strongly. Thus, we studied only the reaction path to 3MP (methyl group at C3) over M(211) surfaces. Over M(211) surfaces the structures of the reactants are quite similar to those over M(111), except that the metal atoms that directly interact with the hydrocarbon are terrace edge atoms on (211) surfaces (Figure 2b). In addition, in the FSs on Rh(211) and Ir(211), the hydrogen-releasing carbon center is bound to two metal atoms at a step edge in a bridge fashion rather than at a top site, as is the case for the other M(211) surfaces and M(111) in general. Bridge-type adsorption was also reported for another monoradical hydrocarbon species (CH_3) on Rh(211).[50] Compared to the dehydrogenation over (111) surfaces, the unsaturated edge atoms interact stronger with the hydrocarbon. For example, in the ISs, the shortest H−M distance is only 179 pm which is 29 pm shorter than in the analogous IS over M(111). The calculated activation barriers of D1 on the M(211) surfaces considered are in the range of 35−60 kJ mol^{-1}, that is, 30−35 kJ mol^{-1} lower than the values on M(111) (Table 1).

Other Dehydrogenation Steps over M(111) Surfaces. Earlier computational studies[43−45,51−54] showed that on Pt, Pd, and Rh metal catalysts the activation energies of ±H reactions, analogous to those discussed in the present work, fall in a narrow range of values. For example, the ±H barriers on Pt surfaces are mostly close to 80 kJ mol^{-1}.[45,51,52] The same reactions over Pd surfaces generally have slightly higher barriers, most of them under 100 kJ mol^{-1}.[43,44,53] Much lower barriers were reported for ±H reactions over the Rh(111) surface.[54] We assume that on other metal surfaces considered herein the highest barriers of ±H reactions are close to that of the first −H reaction. We checked this assumption by calculating the barriers of the second (D2) and third (D3) dehydrogenation steps on the way to *n*Hx. Most of the D2 and D3 barriers are below 70 kJ mol^{-1} (i.e., below the barriers calculated for D1, as expected) except reaction D3 on Pd(111) (Table 1). The latter barrier was calculated at 109 kJ mol^{-1}, 17 kJ mol^{-1} above the barrier for D1. However, as the C−C breaking barrier on the way to *n*Hx is as high as 134 kJ mol^{-1} on Pd(111) (see below), D3 is most likely not the rate-determining step for the overall conversion.

3.2. C−C Bond Breaking Reactions. After a sequence of dehydrogenation reactions (see ref 36. for details), one arrives at two types of intermediates: (i) $\alpha\alpha\beta\beta$-tetra-adsorbed 3-methylcyclopentyne and 4-methylcyclopentyne as well as (ii) $\alpha\alpha\beta$-triadsorbed 2-methyl-1-cyclopenten-1-yl. The former two intermediates ultimately convert to 2MP and 3MP, respectively, whereas the latter intermediate converts to *n*Hx. In the following, we will discuss C−C bond breaking of the $\alpha\alpha\beta\beta$-tetra-adsorbed intermediate (tetra-dehydrogenated, a precursor of 3MP) and of the $\alpha\alpha\beta$-triadsorbed intermediate (tridehydrogenated, a precursor of *n*Hx), separately for flat and stepped metal surfaces.

C−C Bond Breaking on the Reaction Path to 3MP on M(111). In the IS, the ring structure of 4-methylcyclopentyne is oriented almost normal to the surface and the C−C bond to be broken is located above a 3-fold hollow site so that one M atom forms bonds to both C atoms and the other two M atoms form one C−M bond each. We further refer to this adsorption arrangement as parallel bridge mode (‖-bridge, Figure 3). On Pt(111),[36] the actual C−C bond scission of the tetra-dehydrogenated intermediate is preceded by a migration step in which the adsorption geometry of the hydrocarbon changes to a "μ-bridge" mode, where two C atoms occupy two contiguous 3-fold sites with the molecular plane bisecting a M−M bond (μ-bridge, Figure 3). The structural details of the IS and the FS of the migration step on the other metal surfaces studied are quite similar to those on Pt(111).[36] However, the TS structures differ between second- and third-row transition metals (Figure 4). On Rh(111) and Pd(111), the TS structure is closer to the IS, with two C atoms still sharing the same hollow site, whereas the TS on Ir(111) and Pt(111) is more product-like, with the two C atoms occupying neighboring hollow sites. The activation energies of this reaction vary strongly among the four metals. Second-row transition metals feature lower barriers (Rh: 11 kJ mol^{-1}, Pd: 14 kJ mol^{-1}) than third-row transition metals (Ir: 41 kJ mol^{-1}, Pt: 61 kJ mol^{-1}; Table 1). On Pd(111) and Pt(111), the barriers of reverse migration are less than 3 kJ mol^{-1}.

For the subsequent C−C scission step, we do not see any correlation of the activation barriers with the position of the metal in the periodic table. The reaction over Pd(111) has the

dx.doi.org/10.1021/cs3005924 | ACS Catal. 2013, 3, 196−205

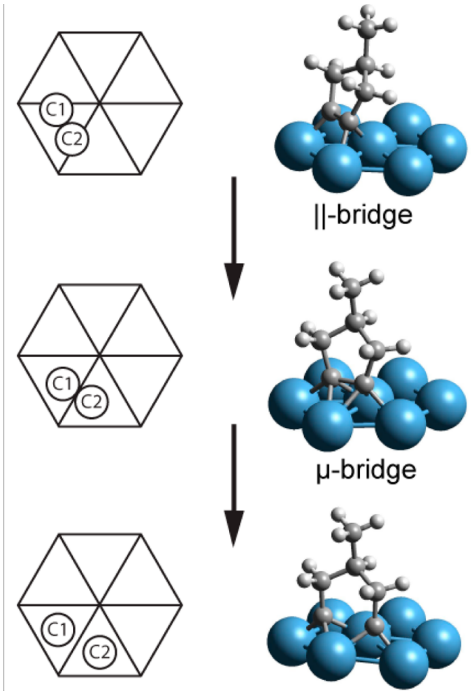

Figure 3. Optimized initial and final structures and a schematic illustration of the adsorption modes during migration and C−C bond breaking on the way to 3MP over Pt(111). The labels C1 and C2 denote the two carbon atoms which are directly bound to the metal surfaces.

highest barrier, 59 kJ mol^{-1}. The barriers on the other three metals are much lower, 14−17 kJ mol^{-1}. However, on Pt(111), Pd(111), and Rh(111), in view of the low reverse barrier of the preceding migration step, the total barrier of the C−C scission should be calculated relative to the most stable configuration of the tetra-adsorbed cyclic species, that is, yielding the energetic cost as the reaction energy of the migration step plus the barrier of C−C cleavage. In contrast, on Ir(111) the migration step is rate-determining and, therefore, the apparent barrier is that of the migration step; for a detailed discussion see the Supporting Information. Thus, the overall barriers become 74 kJ mol^{-1} over Pt(111), 70 kJ mol^{-1} over Pd(111), 18 kJ mol^{-1} over Rh(111), and 41 kJ mol^{-1} over Ir(111).

C−C Bond Breaking on the Reaction Path to 3MP on M(211). The stepped M(211) surface offers more possibilities for adsorption sites and the relative orientation of the dehydrogenated C_6 species undergoing C−C bond scission. We follow the reaction route previously identified,[36] with the tetra-dehydrogenated intermediate adsorbed in a ||-bridge fashion close to the terrace edge (Figure 5a). It turned out that, only on the third-row transition metals, Pt and Ir, ring cleavage can proceed directly from a ||-bridge adsorbed IS (Figure 5a) with activation barriers of 102 kJ mol^{-1} and 89 kJ mol^{-1}. On Rh(211) and Pd(211), the adsorbate needs to change to μ-bridge adsorption before the C−C bond breaks, with relatively low barriers, less than 22 kJ mol^{-1} (Figure 5b). Interestingly, on Ir(211) in addition to the direct path, a similar two-step pathway was also identified, with a higher migration barrier, 66 kJ mol^{-1}, than on Rh and Pd. Characteristic for this site-change step is a very low barrier of the reverse process, only 3 kJ mol^{-1} on Rh(211) and Pd(211) and less than 0.5 kJ mol^{-1} on Ir(211). Such extremely low barriers for transformations to more stable ||-bridge modes rationalize the difficulty we

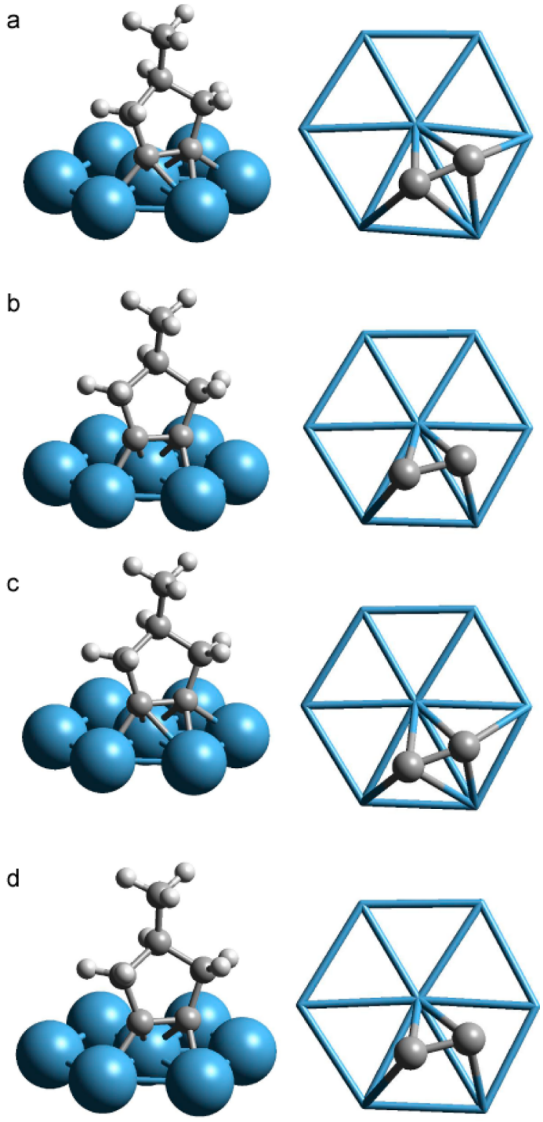

Figure 4. Optimized transition state structures for the migration step on the reaction path to 3MP over (a) Pt(111); (b) Rh(111); (c) Ir(111); (d) Pd(111). Only C centers that directly connect to the surface are shown in the top view.

experienced in locating μ-bridge structures on these surfaces. On Pt(211) the μ-bridge adsorbed intermediate was calculated unstable. The activation energy of the C−C scission step following the transformation to μ-bridge mode thus has to be combined with the reaction energy of the preceding migration step, resulting in the overall barriers of 86 kJ mol^{-1} on Pd(211), 77 kJ mol^{-1} on Ir(211), and 46 kJ mol^{-1} on Rh(211).

Note that the final states of C−C scission are slightly different for direct and stepwise pathways. In the FSs of direct C−C cleavage on Pt(211) and Ir(211), one of the dissociated C atoms remains directly bound to the step edge in a 2-fold fashion (Figure 5a), as in the corresponding ISs, whereas the RO of a μ-bridge adsorbed intermediate on Rh(211), Pd(211), and Ir(211) results in structures where both terminal C atoms move to 3-fold hollow sites (Figure 5b).

C−C Bond Breaking on the Reaction Path to nHx on M(111). This step on M(111) proceeds via a similar reaction path as on Pt(111),[36] from a μ_3-η^2 adsorbed IS to a FS with the two terminal C atoms at a bridge and a hollow site (Figure 6a).

dx.doi.org/10.1021/cs3005924 | *ACS Catal.* 2013, 3, 196−205

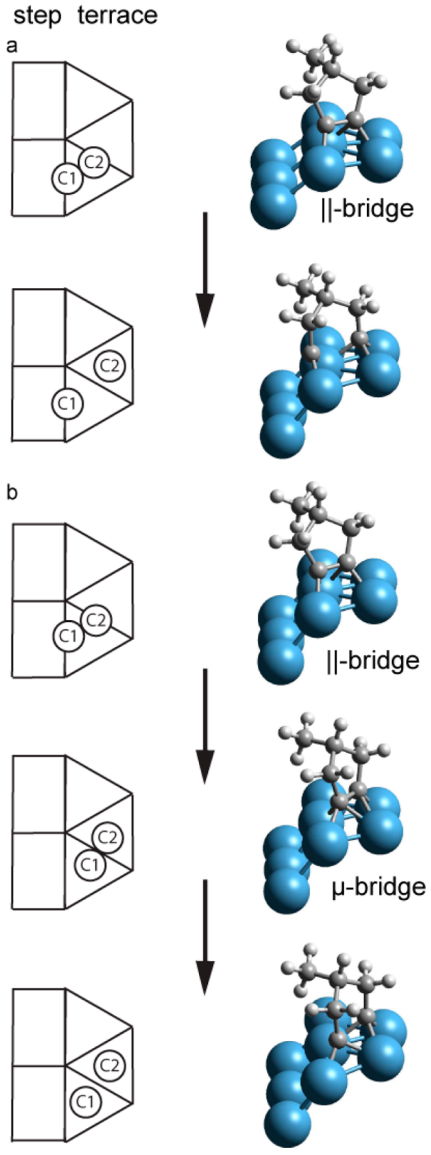

Figure 5. Optimized initial and final structures and a schematic illustration of the adsorption modes for the migration and C−C bond scission on the way to 3MP; (a) direct C−C bond scission over Pt(211), and (b) stepwise path, migration followed by C−C bond scission, over Rh(211). Lay-out as in Figure 3.

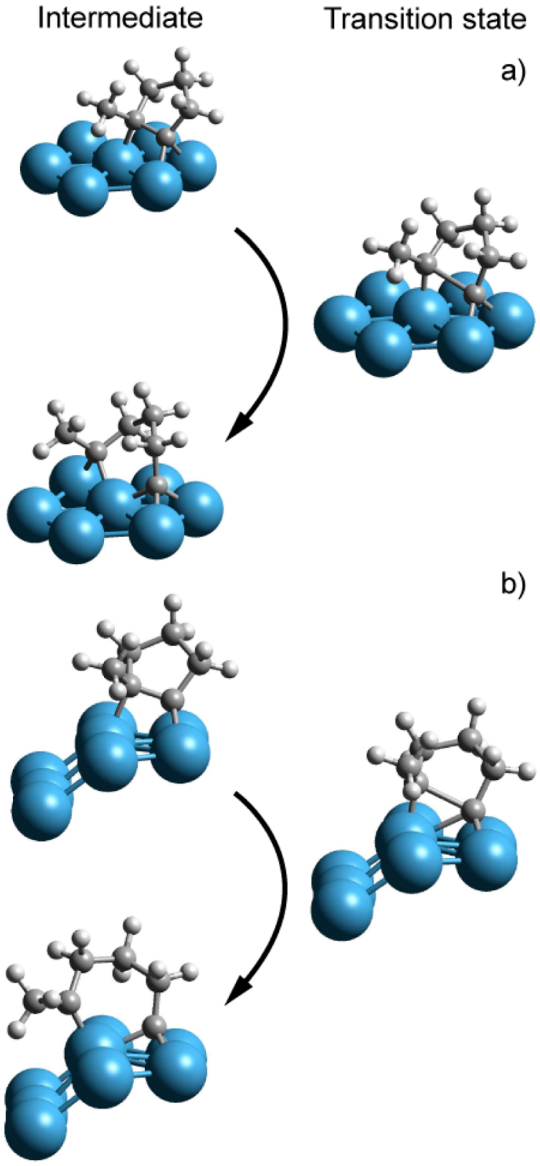

Figure 6. Optimized structures of the C−C bond scission step on the reaction path to *n*Hx over (a) Pt(111); (b) Pt(211).

A relatively high C−C scission barrier is calculated for the reaction over Pd(111), 134 kJ mol^{-1}, and Pt(111), 116 kJ mol^{-1}. Lower barriers were obtained over Rh(111), 70 kJ mol^{-1}, and Ir(111), 62 kJ mol^{-1}.

C−C Bond Breaking on the Reaction Path to nHx on M(211). On M(211) the structural arrangements of the ISs and TSs are rather similar to those on M(111), while in the FSs the dissociating C center with the methyl group attached forms only one C−M bond with a terrace edge atom (Figure 6b). The calculated barrier heights are lower than the values calculated for M(111). The highest barrier is still found for Pd, 119 kJ mol^{-1}. The barriers on Pt(211), Rh(211), and Ir(211) are 94, 59, 38 kJ mol^{-1}, respectively.

4. DISCUSSION

In the following, we will analyze the results of the calculations described in Section 3. We will focus on the catalytic activity of the four metals, and we will try to correlate it with experimental observations on the selectivity of SRO products for each metal catalyst. The calculated energy profiles of the first dehydrogenation step and the C−C scission, including the preceding migration step, are compared in the Supporting Information.

4.1. Catalytic Activity. *C−H Activation.* All selected metal surfaces were reported to catalyze C−H bond cleavage. For example, ethylene was observed to be easily converted to ethylidyne on Pt(111),[55] and Pd(111)[56] near room temperature via several steps of ±H reactions. In the present study, the calculated barriers for the dehydrogenation steps of MCP on M(111) are not very high, mostly less than 90 kJ mol^{-1}. For these dehydrogenation steps, the barriers from low to high on different metals follow the trend: Ir(111) < Rh(111) < Pt(111) < Pd(111) (Table 1, Supporting Information, Figure S1) which correlates with the calculated activity of methane dehydrogenation,[57] and the experimental conversion temperature of ethylene to ethylidyne, 180 K on Ir(111),[58] 190 K on Rh(111),[59] 250 K on Pt(111),[55] and 300 K on Pd(111),[56] as

dx.doi.org/10.1021/cs3005924 | *ACS Catal.* 2013, 3, 196−205

well as with the activity of the MCP RO reactions, Ir ≈ Rh > Pt > Pd.[12]

On the stepped M(211) surfaces, the barriers of D1 range from 35 kJ mol^{-1} on Ir(211) to 60 kJ mol^{-1} on Pd(211). This interval is shifted downward by about 30 kJ mol^{-1} relative to the barriers on M(111) (Table 1, Supporting Information, Figure S1). A similar barrier lowering at stepped surfaces was also determined for the dehydrogenation of methane on Rh surfaces,[50] and of propane[51] or ethane[60] on Pt surfaces. One can readily rationalize why dehydrogenation barriers on stepped surfaces are lower. In the IS, saturated hydrocarbons are physically adsorbed on the surface. The adsorption energies are similar on M(111) and M(211) (Supporting Information, Figure S1). However, in the TS, the hydrocarbon is already chemically bound to a metal atom at the step edge of the surface. This bond is stronger on M(211) than the corresponding bond on the flat M(111) surface, resulting in a lower TS energy at the stepped surface.

Adsorption Modes of the Tetra-Dehydrogenated Intermediate. Before the C−C bond breaking of the tetra-dehydrogenated intermediate occurs on M(111), Rh(211) and Pd(211), a migration step is required to change the adsorption mode from a ‖-bridge to μ-bridge. On Ir(211), RO can proceed either directly from a ‖-bridge structure or via a μ-bridge intermediate. In the latter geometry, the interaction between metal s states and the π^* orbital of the C−C bond weakens the C−C bond,[61] facilitating the subsequent C−C bond scission. This weakening in the μ-bridge on M(111) is reflected in an elongation of the C−C bond by 3−11 pm compared to the length of the same bond in the ‖-bridge mode on M(111).

Generally, on the M(111) surfaces studied, the intermediate adsorbed via a μ-bridge is only slightly less favorable, by 2−23 kJ mol^{-1}, compared to the ‖-bridge mode (Table 2). However,

Table 2. Binding Energies (kJ mol^{-1}) of Tetra-Dehydrogenated 3-Methylcyclopentyne over M(111) and M(211) Surfaces

	Pt		Pd		Ir		Rh	
adsorption mode	111	211	111	211	111	211	111	211
‖-bridge	491	499	438	444	515	536	490	499
μ-bridge[a]	431		427	442	492	470	488	480

[a]The μ-bridge adsorption mode is unstable on Pt(211).

on Pt(111), the adsorption energy of the μ-bridge mode is significantly lower, by 60 kJ mol^{-1}, than the adsorption energy of the ‖-bridge; the conversion from μ-bridge to ‖-bridge occurs essentially without barrier on Pt(111) (only 1 kJ mol^{-1}). This result concurs with the conclusions of an earlier theoretical study on acetylene adsorption at Pt(111)[61] which determined the μ-bridge mode as unstable. The authors further rationalized this phenomenon by the weakened interaction between metal s states and C−C antibonding states when moving down the periodic table.[61] The migration barriers calculated here for moving from ‖-bridge to μ-bridge rank in the order Rh(111) < Pd(111) < Ir(111) < Pt(111). The higher activation barriers for Ir and Pt correlate with the higher endothermicity of this rearrangement (23 and 60 kJ mol^{-1}) compared with the values obtained for Rh and Pd (2 and 11 kJ mol^{-1}), Table 1.

On Pt(211) and Ir(211), the μ-bridge adsorbed tetra-dehydrogenated intermediate was calculated either unstable or metastable, converting essentially without barrier to ‖-bridge mode. This could be due to stronger binding between the C centers and the step-edge metal atoms than on the flat surface. This is also reflected in the product state of the direct C−C cleavage on Pt(211) and Ir(211) by only 2-fold coordination of the carbyne type C center adsorbed on the step edge, which is the same mode as in the ‖-bridge complex, whereas on M(111) surfaces carbynic C prefers 3-fold coordination.

C−C Activation. The calculated barriers of C−C bond breaking vary stronger among the four metals considered than the barriers of ±H reactions discussed above. In general, ring cleavage of the tridehydrogenated 2-methyl-1-cyclopenten-1-yl intermediate was determined to have a higher barrier compared to the analogous reaction of the tetra-dehydrogenated 4-methylcyclopentyne intermediate over M(111). This result is in line with the expectation that removal of an additional H atom should enhance the interaction between C atoms and metal surface, thus lowering the barrier for C−C cleavage. A similar conclusion was reached in a study on propane decomposition at Pt(111)[51] which determined a significantly lower C−C scission barrier for $\alpha\alpha\beta\beta$-tetra-adsorbed propyne than for the $\alpha\alpha\beta$-triadsorbed species CH_3CCH_2 and CH_3CHCH.

The lower barrier for C−C bond breaking from a $\alpha\alpha\beta\beta$-tetra-adsorbed intermediate than from a $\alpha\alpha\beta$-triadsorbed intermediate can be rationalized by a more stabilized transition state for the ring-opening of a tetra-dehydrogenated intermediate or, in other words, by a flatter potential energy surface. In the initial state of this reaction, which on M(111) proceeds from the μ-bridge adsorbed intermediate, the hydrocarbon ring is attached to two adjacent 3-fold hollow sites, with each of the two binding C atoms bound over one hollow site. The C−C bond length in the initial state is typical for a C−C single bond, about 150 pm. In the transition state structures, this distance notably increases, by 10−20 pm, as the C atoms move toward the centers of the respective hollow sites. Therefore, in the initial and transition states of the ring-opening, the bonding interactions between the C and surface Pt atoms should be similar due to the similar adsorption mode of the C centers. Moreover, the hollow site is the most stable site for the adsorption of a carbyne species on M(111) surfaces. In contrast, the C−C bond breaking of a tridehydrogenated intermediate passes via a transition state where one of the reactive C atoms moves to a top site which is *not* the most stable one (bridge site) for a carbene species. In addition, the displacements of the reacting C atoms along the whole transformation from the initial state to the final state are much larger in this case than during C−C breaking in tetra-dehydrogenated intermediates. In that latter reaction, the C−C distance in the transition state on various metals is only 175−196 pm, which is shorter than a typical C−C distance in a transition state for C−C activation, >200 pm.[62] Even in the final state of the dissociation, the C−C distance is still only 224−237 pm, notably shorter than the distance between the dissociated C centers in the final state of the reaction from a tridehydrogenated intermediate, ∼300 pm. Thus, the activation barrier of C−C breaking in a tetra-dehydrogenated intermediate, both with a flatter potential energy surface and a shorter reaction path, should be lower than that of C−C breaking in a tridehydrogenated intermediate.

On the M(211) surface, the barriers for C−C cleavage of the tridehydrogenated intermediate are lower by 11−24 kJ mol^{-1} compared to the reaction on M(111). This lowering likely is because on M(211) the ISs are slightly less stable compared to

dx.doi.org/10.1021/cs3005924 | ACS Catal. 2013, 3, 196−205

those on M(111) (Supporting Information, Figure S3b). Also, in the TSs, the singly adsorbed C atom with the methyl substituent is attached to a terrace edge metal atom which is coordinatively less saturated than the atoms of the M(111) surface and, thus, the TS structure is stabilized through an enhanced interaction of the hydrocarbon with the terrace edge atoms of the metal catalyst. In contrast, the barriers for ring cleavage of the tetra-dehydrogenated intermediates increase on M(211) compared to M(111). In these cases, the stabilization due to unsaturated terrace edge atoms is more dominant in the ISs. On M(211), the BE of ISs are 10−21 kJ mol^{-1} larger than on the corresponding (111) surfaces (Supporting Information, Figure S3a). At the same time, the TSs are destabilized compared to the corresponding ones on M(111) (Supporting Information, Figure S3a) because of competition between two stable adsorption sites, the hollow site and the unsaturated edge-bridge site.

4.2. Particle-Size Effect. Extensive experimental research on MCP RO summarized in ref 6 has shown that the catalyst dispersion is one of the main factors that affect the RO product distribution. For example, large Pt particles selectively produce branched 2MP and 3MP with the formation of *n*Hx being suppressed.[18] On the other hand, small Pt particles non-selectively produce a statistical mixture of 2MP, 3MP, and *n*Hx.[19] However, on other metals, like Rh[21,27] or Ir,[12,19,20] 2MP and 3MP are selectively produced irrespective of the particle size. These phenomena can be readily interpreted in terms of the calculated activation energies of the key reaction steps on the planar M(111) and stepped M(211) surfaces. In a previous study,[36] we discussed in detail the particle size effect for Pt-based catalysts. Therefore, we will focus on the Rh-, Ir-, and Pd-based catalysts in the following.

Rh-Based Catalysts. Unlike Pt, Rh catalysts exhibit a higher propensity for selectively opening the five-member ring in the unsubstituted positions, producing predominantly branched 2MP and 3MP. Del Angel et al.[21] carried out a series of MCP RO experiments using Rh supported on silica or alumina with varying metal loading (0.11−1.4%). In most cases, the selectivity to *n*Hx was less than 4.5% with the exception of well-dispersed Rh/Al_2O_3, on which the selectivity for *n*Hx increased to 10%. On the other hand, the produced 2MP and 3MP were obtained in a ratio close to 2:1, which represents the statistical value for breaking unsubstituted C−C bonds. Similar trends were observed by Teschner et al.[27] in a study of MCP RO on 0.3%, 3%, and 10% Rh loaded catalysts supported on alumina. According to the results of our calculations, presented in Section 3, ring cleavage of tetra-dehydrogenated intermediates at unsubstituted positions is very facile on both Rh(111) and Rh(211), only 18 kJ mol^{-1} and 46 kJ mol^{-1}, respectively. In contrast, pathways to *n*Hx exhibit much higher C−C scission barriers, 70 kJ mol^{-1} on Rh(111) and 59 kJ mol^{-1} on Rh(211). Independent of the surface morphology, C−C bond scission barrier to the branched product 3MP (and 2MP) is lower than the barrier to *n*Hx; thus formation of *n*Hx is less probable on both surfaces, which well explains the experimental observations.[21,27]

Ir-Based Catalysts. According to experiment, the selectivity of Ir-based catalysts is also not affected by the particle size of the metal, with the selectivity always toward branched hexanes, 2MP or 3MP.[12,19,20] Sárkány reported[20] that the RO of MCP catalyzed by large Ir particles (10 wt % Ir/Al_2O_3) yielded 2MP, 3MP, and *n*Hx at a ratio of 64:32:3. Similarly low selectivity toward *n*Hx, < 5%, was recently reported using smaller Ir particles by Samoila et al.[12] (0.6 wt % Ir/Al_2O_3) and by McVicker et al.[19] (0.9 wt % Ir/Al_2O_3). Again, our calculated results can well explain the observed selective splitting of unsubstituted C−C bonds on large Ir particles. On Ir(111), the reaction from the tetra-dehydrogenated intermediate has to overcome a barrier of 41 kJ mol^{-1} in the migration step. The subsequent C−C scission encounters a very low barrier of only 17 kJ mol^{-1}. Both values are at least 21 kJ mol^{-1} lower than the activation energy for C−C bond breaking in the tridehydrogenated intermediate, the precursor of *n*Hx. Therefore, just as on Pt(111) and Rh(111), the selectivity toward *n*Hx is predicted to be low on Ir(111) as well as over terrace-rich large Ir particles. On Ir(211), the calculated C−C bond scission barrier for the tridehydrogenated intermediate decreases to 38 kJ mol^{-1}. This value is not only notably lower, 39 and 51 kJ mol^{-1}, than the barriers for stepwise and direct C−C scission, respectively, in the tetra-dehydrogenated intermediate over Ir(211) (see Supporting Information, Figure S3), but also comparable with the barrier of the migration step of the tetra-dehydrogenated intermediate on Ir(111). However, our results, Supporting Information, Figure S3a, also suggest that step-edge hollow sites on Ir(211) should be blocked by tetra-dehydrogenated species adsorbed in ‖-bridge fashion because these sites offer an additional stabilization of 21 kJ mol^{-1} for these species over terrace fcc hollow sites. In addition, possible exit channels have rather high activation barriers: at least 66 kJ mol^{-1} for migration to a terrace 3-fold site via a μ-bridge and even 89 kJ mol^{-1} for direct C−C scission. Both barriers are much higher than all other barriers of C−C scission (<41 kJ mol^{-1}) on Ir(211) and Ir(111). Therefore, production of *n*Hx is still depressed on small defect-rich Ir particles. In contrast, the step sites on Pt(211) do not get blocked because the C−C scission barrier of the tetradehydrogenated intermediate, ∼100 kJ mol^{-1}, is only slightly above the barrier, 94 kJ mol^{-1}, of the energetically preferred pathway to *n*Hx (Supporting Information, Figure S3). Thus, all three isomeric hexanes can form at step edges of Pt catalysts. Note that the RO reaction on Pt-based catalysts requires a higher temperature (∼620−650 K) than on Ir (∼550−575 K),[12,19] reflecting the higher activation barriers on Pt.

Pd-Based Catalysts. Because of the relatively low activity of Pd-based catalysts for MCP RO, they were not explored by experiment as extensively as Pt-, Rh-, and Ir-based ones. Le Normand et al.[22] found no change in the relative selectivity of RO products when using Pd/Al_2O_3 catalysts with Pd particle diameters between 1.5 and 12 nm. The selectivity to *n*Hx was in a narrow range, 18%−24.5%, and branched hexanes (2MP, 3MP) were preferentially formed. Again, this preference is consistent with the barriers calculated here for C−C bond scission of tri- and tetra-dehydrogenated cyclic intermediates. The barrier for C−C cleavage on the reaction path to 3MP is 70 kJ mol^{-1} on Pd(111), which is 64 kJ mol^{-1} lower than the barrier for the same step on the reaction path to *n*Hx. Similarly, on Pd(211) the barrier for ring-opening to the precursor of 3MP was calculated 35 kJ mol^{-1} lower than the analogous reaction to the precursor of *n*Hx. The higher barrier of C−C scission on the way to *n*Hx is in agreement with its lower yields on both terrace and defect sites; however, according to our calculated activation energies, *n*Hx should not be formed at all on Pd because of very high barriers calculated, 134 kJ mol^{-1} for Pd(111) and 111 kJ mol^{-1} for Pd(211). These values are also well above the barriers for ±H reactions, Table 1. Hence, our currently assumed mechanism is not able to rationalize the

dx.doi.org/10.1021/cs3005924 | ACS Catal. 2013, 3, 196−205

relatively high yield of *n*Hx observed in experiment.[22] Other side reactions, including those on the oxide support, could lead to the increased selectivity toward *n*Hx. For example, the formation of *n*Hx on Pd/Al_2O_3 was reported to be significantly enhanced after high-temperature pretreatment which served to increase Lewis acidity of the carrier.[63] On the more active metals considered above, the reactions involving the acidic support do not affect the product distribution to a significant extent since they are much slower than the RO reaction on the metal particles.

Final Comments. We addressed particle-size effects on the RO selectivity of MCP on the basis of our proposed mechanism which involves tri- and tetra-dehydrogenated MCP derivatives. This mechanism allows one to rationalize successfully particle size effects on Pt, Rh, Ir, and Pd-based catalysts.

On the basis of activation barriers calculated for Pt(111), we preferred the "dissociative" mechanism in which deep dehydrogenation of two neighboring C centers precedes ring cleavage.[36] In the present work, we assumed that the same route is also followed on other noble metals. However, this may not necessarily be the case. For example, Teschner et al.[29] examined the effect of hydrogen pressure on the MCP RO reaction using Rh-based catalysts. They observed that RO reactions show a positive order in the partial pressure of hydrogen which indicates that the dehydrogenation of the intermediate was not very deep. Le Normand et al.[22] proposed a mechanism on Pd-based catalysts which only requires one dehydrogenation step before C−C bond breaking. A statistical distribution of the products through this mechanism would be 2MP:3MP:*n*Hx = 50:25:25, which is quite close to their experimental observations. In contrast to the above, in this work, we assumed the C−C scission step, which apparently is decisive for the selectivity, to take place after complete dehydrogenation of the adsorbed C centers. However, one cannot exclude that other mechanisms, for example, C−C scission from partially dehydrogenated intermediates or an $\alpha\gamma$-intermediate,[7] could come into play on some of the metals considered.

The second remark concerns hydrogenation/dehydrogenation reactions. Although some barriers of the first dehydrogenation reactions (D1) were calculated higher than the migration or C−C scission barriers on several surfaces, we did not consider them to be important to the selectivity of RO products because, on the same metal surface, the barriers of the same dehydrogenation step to the three hexane isomers are very close to each other. Thus, similar reaction rates of dehydrogenation are expected on the way to the three hexane isomers. Nevertheless, the ±H barriers may in some cases be decisive for the overall activity of a catalyst.

We also would like to comment briefly on coverage effects. The DFT results of this work were obtained assuming 1/9 coverage of the hydrocarbon on the surface. At different coverage, the activation energies of ±H reactions may change by up to 25 kJ mol^{-1} as the effective coverage changes during the reaction.[45] A strong coverage effect is also expected for the C−C scission steps (including migration and C-shift steps) where the effective coverage increases during the reaction. Because in most experimental studies of MCP RO reaction H_2 is supplied in excess, the surface is expected to be saturated by H atoms and hence the barriers could significantly deviate from those predicted in our model study because of the change of the surface coverage. A more reliable way to address the reaction kinetics theoretically would be to perform kinetic Monte Carlo simulations using our calculated barriers, which allows one to take into consideration actual reaction conditions, including the effect of surface coverage, temperature of the system, and pressure of the gas-phase reactants.

5. CONCLUSIONS

We studied computationally the conversion of methylcyclopentane (MCP) to its ring-opening (RO) products 2MP, 3MP, and *n*Hx over the catalyst surfaces M(111) and M(211), M = Pt, Rh, Ir, and Pd. We calculated the transition state structures and activation energies for the C−C scission step, which we suggest to be important for the selectivity. In addition, we studied selected dehydrogenation steps to gain a basic idea about how the corresponding barrier heights vary with the metal.

Our computational results show that barriers for analogous dehydrogenation steps follow the trend: Ir(111) < Rh(111) < Pt(111) < Pd(111). The barrier heights for C−C rupture from low to high follow the trend Rh < Ir < Pt < Pd, which is similar to the experimentally observed activity of these catalysts for MCP ring-opening, Rh ≈ Ir < Pt < Pd, with the exception of the relative order of Rh and Ir.[12] However, the overall activity also depends on the barrier heights of ±H reactions, some of which were not calculated in this study.

On the basis of the calculated barriers for C−C bond scission, we were able to rationalize the particle-size effect on the RO product distribution (2MP, 3MP, and *n*Hx) catalyzed by these metals. The selectivity of the RO products correlates with the height of the C−C scission barrier at terrace or step edge sites. The generally good agreement between our calculations and experimental evidence suggests that the proposed mechanism likely is dominant in reality.

Notwithstanding the evident success of our present model in the rationalization of the experimental activity patterns for the four noble-metal catalysts, one should keep in mind that several other plausible pathways have not been considered in this work, for example, the metallocyclobutane mechanism.[7] In contrast, the "multiplet" mechanism,[26] requiring flat adsorption of the five-member ring, seems rather unlikely in view of the present results and those of our preceding work,[36] which show that at least partial dehydrogenation of C atoms interacting with the metal surface should occur prior to C−C cleavage. Our present model neglected any direct involvement of the support. However, the acidic support could play a notable role such that ring-opening may simultaneously proceed on the metal and the acidic centers.

■ ASSOCIATED CONTENT

Supporting Information

Energy profiles of the reaction over various metals; rate expression for a two-step reaction with an unstable intermediate; Cartesian coordinates of the most significant intermediates and transition states. This material is available free of charge via the Internet at http://pubs.acs.org.

■ AUTHOR INFORMATION

Corresponding Author

*E-mail: roesch@mytum.de.

Notes

The authors declare no competing financial interest.

■ ACKNOWLEDGMENTS

Z.J.Z. gratefully acknowledges financial support by the International Doctorate Program NanoCat within the Bavarian Network of Excellence, an associated member of the TUM Graduate School at Technische Universität München. This work was supported by Deutsche Forschungsgemeinschaft and Fonds der Chemischen Industrie (Germany). We also acknowledge generous computing resources at Leibniz Rechenzentrum München.

■ REFERENCES

(1) Jacobson, M. Z. *J. Geophys. Res.* **2002**, *107*, 4410.
(2) Gaffney, J. S.; Marley, N. A. *Atmos. Environ.* **2009**, *43*, 23.
(3) Santana, R. C.; Do, P. T.; Santikunaporn, M.; Alvarez, W. E.; Taylor, J. D.; Sughrue, E. L.; Resasco, D. E. *Fuel* **2006**, *85*, 643.
(4) Stanislaus, A.; Cooper, B. H. *Catal. Rev.—Sci. Eng.* **1994**, *36*, 75.
(5) Scherzer, J.; Gruia, A. J. *Hydrocracking Science and Technology*; Marcel Dekker: New York, 1996.
(6) Du, H.; Fairbridge, C.; Yang, H.; Ring, Z. *Appl. Catal., A* **2005**, *294*, 1.
(7) Gault, F. G. *Adv. Catal.* **1981**, *30*, 1.
(8) Hagedorn, C. J.; Weiss, M. J.; Kim, T. W.; Weinberg, W. H. *J. Am. Chem. Soc.* **2001**, *123*, 929.
(9) Do, P. T.; Alvarez, E.; Resasco, D. E. *J. Catal.* **2006**, *238*, 477.
(10) Kalakkad, D.; Anderson, S. L.; Logan, A. D.; Pena, J.; Braunschweig, E. J.; Peden, C. H. F.; Datye, A. K. *J. Phys. Chem.* **1993**, *97*, 1437.
(11) Győrffy, N.; Bakos, I.; Szabó, S.; Tóth, L.; Wild, U.; Schlögl, R.; Paál, Z. *J. Catal.* **2009**, *263*, 372.
(12) Samoila, P.; Boutzeloit, M.; Especel, C.; Epron, F.; Marécot, P. *Appl. Catal., A* **2009**, *369*, 104.
(13) Wang, Z.; Nelson, A. E. *Catal. Lett.* **2008**, *123*, 226.
(14) Chimentão, R. J.; Valença, G. P.; Medina, F.; Pérez-Ramírez, J. *Appl. Surf. Sci.* **2007**, *253*, 5888.
(15) Rao, R. N.; You, N.; Yoon, S.; Upare, D. P.; Park, Y.-K.; Lee, C. W. *Catal. Lett.* **2011**, *141*, 1047.
(16) Poupin, C.; Pirault-Roy, L.; La Fontaine, C.; Tóth, L.; Chamam, M.; Wootsch, A.; Paál, Z. *J. Catal.* **2010**, *272*, 315.
(17) Győrffy, N.; Wootsch, A.; Szabó, S.; Bakos, I.; Tóth, L.; Paál, Z. *Top. Catal.* **2007**, *46*, 57.
(18) Maire, G.; Plouidy, G.; Prudhomme, J. C.; Gault, F. G. *J. Catal.* **1965**, *4*, 556.
(19) McVicker, G. B.; Daage, M.; Touvelle, M. S.; Hudson, C. W.; Klein, D. P.; Baird, W. C., Jr.; Cook, B. R.; Chen, J. G.; Hantzer, S.; Vaughan, D. E. W.; Ellis, E. S.; Feeley, O. C. *J. Catal.* **2002**, *210*, 137.
(20) Sárkány, A. *J. Chem. Soc., Faraday Trans. 1* **1989**, *85*, 1523.
(21) Del Angel, G.; Coq, B.; Dutartre, R.; Figueras, F. *J. Catal.* **1984**, *87*, 27.
(22) Le Normand, F.; Kili, K.; Schmitt, J. L. *J. Catal.* **1993**, *139*, 234.
(23) Espinosa, G.; Del Angel, G.; Barbier, J.; Bosch, P.; Lara, V.; Acosta, D. *J. Mol. Catal. A* **2000**, *164*, 253.
(24) Samoila, P.; Boutzeloit, M.; Especel, C.; Epron, F.; Marécot, P. *J. Catal.* **2010**, *276*, 237.
(25) Teschner, D.; Pirault-Roy, L.; Naud, D.; Guérin, M.; Paál, Z. *Appl. Catal., A* **2003**, *252*, 421.
(26) Hayek, K.; Kramer, R.; Paál, Z. *Appl. Catal., A* **1997**, *162*, 1.
(27) Teschner, D.; Matusek, K.; Paál, Z. *J. Catal.* **2000**, *192*, 335.
(28) Van Senden, J. C.; Broekhoven, E. H.; Wreesman, C. T. J.; Ponec, V. *J. Catal.* **1984**, *87*, 468.
(29) Teschner, D.; Paál, Z.; Duprez, D. *Catal. Today* **2001**, *65*, 185.
(30) Bai, X.; Sachtler, W. M. H. *J. Catal.* **1991**, *129*, 121.
(31) Pallassana, V.; Neurock, M. *J. Catal.* **2000**, *191*, 301.
(32) Neurock, M.; van Santen, R. A. *J. Phys. Chem. B* **2000**, *104*, 11127.
(33) Jones, G.; Jakobsen, J. G.; Shim, S. S.; Kleis, J.; Andersson, M. P.; Rossmeisl, J.; Abild-Pedersen, F.; Bligaard, T.; Helveg, S.; Hinnemann, B.; Rostrup-Nielsen, J. R.; Chorkendorff, I.; Sehested, J.; Nørskov, J. K. *J. Catal.* **2008**, *259*, 147.
(34) Joubert, J.; Delbecq, F.; Sautet, P.; Le Roux, E.; Taoufik, M.; Thieuleux, C.; Blanc, F.; Coperet, C.; Thivolle-Cazat, J.; Basset, J.-M. *J. Am. Chem. Soc.* **2006**, *128*, 9157.
(35) Greeley, J.; Mavrikakis, M. *J. Am. Chem. Soc.* **2004**, *126*, 3910.
(36) Zhao, Z.-J.; Moskaleva, L. V.; Rösch, N. *J. Catal.* **2012**, *285*, 124.
(37) Kresse, G.; Hafner, J. *Phys. Rev. B* **1994**, *49*, 14251.
(38) Kresse, G.; Furthmüller, J. *Comput. Mater. Sci.* **1996**, *6*, 15.
(39) Perdew, J. P.; Wang, Y. *Phys. Rev. B* **1992**, *45*, 13244.
(40) Blöchl, P. E. *Phys. Rev. B* **1994**, *50*, 17953.
(41) Kresse, G.; Joubert, D. *Phys. Rev. B* **1999**, *59*, 1758.
(42) Monkhorst, H. J.; Pack, J. D. *Phys. Rev. B* **1976**, *13*, 5188.
(43) Moskaleva, L. V.; Chen, Z.-X.; Aleksandrov, H. A.; Mohammed, A. B.; Sun, Q.; Rösch, N. *J. Phys. Chem. C* **2009**, *113*, 2512.
(44) Moskaleva, L. V.; Aleksandrov, H. A.; Basaran, D.; Zhao, Z.-J.; Rösch, N. *J. Phys. Chem. C* **2009**, *113*, 15373.
(45) Zhao, Z.-J.; Moskaleva, L. V.; Aleksandrov, H. A.; Basaran, D.; Rösch, N. *J. Phys. Chem. C* **2010**, *114*, 12190.
(46) Methfessel, M.; Paxton, A. T. *Phys. Rev. B* **1989**, *40*, 3616.
(47) Henkelman, G.; Jónsson, H. *J. Chem. Phys.* **1999**, *111*, 7010.
(48) Mills, G.; Jónsson, H.; Schenter, G. K. *Surf. Sci.* **1995**, *324*, 305.
(49) Jónsson, H.; Mills, G.; Jacobsen, K. W. In *Classical and Quantum Dynamics in Condensed Phase Simulations*; Berne, B. J., Ciccotti, G., Coker, D. F., Eds.; World Scientific: Singapore, 1998; p 385.
(50) van Grootel, P. W.; van Santen, R. A.; Hensen, E. J. M. *J. Phys. Chem. C* **2011**, *115*, 13027.
(51) Yang, M.-L.; Zhu, Y.-A.; Fan, C.; Sui, Z.-J.; Chen, D.; Zhou, X.-G. *Phys. Chem. Chem. Phys.* **2011**, *13*, 3257.
(52) Anghel, A. T.; Wales, D. J.; Jenkins, S. J.; King, D. A. *J. Chem. Phys.* **2007**, *126*, 044710.
(53) Chen, Z.-X.; Aleksandrov, H. A.; Basaran, D.; Rösch, N. *J. Phys. Chem. C* **2010**, *114*, 17683.
(54) Basaran, D.; Aleksandrov, H. A.; Chen, Z.-X.; Zhao, Z.-J.; Rösch, N. *J. Mol. Catal. A.: Chem.* **2011**, *344*, 37.
(55) Kesmodel, L. L.; Dubois, L. H.; Somorjai, G. A. *J. Chem. Phys.* **1979**, *70*, 2180.
(56) Kesmodel, L. L.; Gates, J. A. *Surf. Sci.* **1981**, *111*, L747.
(57) Xing, B.; Pang, X.-Y.; Wang, G.-C. *J. Catal.* **2011**, *282*, 74.
(58) Marinova, Ts.; Kostov, K. L. *Surf. Sci.* **1987**, *181*, 573.
(59) Borg, H. J.; van Hardeveld, R. M.; Niemantsverdriet, J. W. *J. Chem. Soc., Faraday Trans.* **1995**, *91*, 3679.
(60) Chen, Y.; Vlachos, D. G. *J. Phys. Chem. C* **2010**, *114*, 4973.
(61) Medlin, J. W.; Allendorf, M. D. *J. Phys. Chem. B* **2003**, *107*, 217.
(62) Cheng, J.; Hu, P.; Ellis, P.; French, S.; Kelly, G.; Lok, C. M. *J. Phys. Chem. C* **2008**, *112*, 6082.
(63) Łomot, D.; Juszczyk, W.; Karpiński, Z. *Appl. Catal., A* **1997**, *155*, 99.